JMEPEG (2004) 13:303-308
DOI: 10.1361/10599490419270

1059-9495/$19.00

Development of Proton Conductors Using Pyrochlore-Perovskite Phase Boundaries

Scott A. Speakman, Robert D. Carneim, E. Andrew Payzant, and Timothy R. Armstrong

(Submitted 1 December 2003)

The pyrochlore-perovskite binary systems $La_2Zr_2O_7$-$SrZrO_3$ and $La_2Zr_2O_7$-$LaYO_3$ were studied as potential high-temperature proton conductors. X-ray diffraction and direct current conductivity measurements were used to develop empirical relationships between structure and conductivity. The solubilities of Sr in $La_2Zr_2O_7$ and La in $SrZrO_3$ were low, less than 0.1 mol fraction. The solubility of Zr in $LaYO_3$ was at least 0.125 mol fraction, and the solubility of Y in $La_2Zr_2O_7$ was at least 0.25 mol fraction. Y-doped $La_2Zr_2O_7$ had the highest electrical conductivity, though no composition exceeded $\sigma = 3 \times 10^{-4}$ S/cm at the target temperature of 600 °C. The effectiveness of Y as a dopant in $La_2Zr_2O_7$ was limited because Y substituted for both La on the A-site and Zr on the B-site.

Keywords conductivity, doping, structure-property relationship, x-ray diffraction

1. Introduction

X-ray diffraction (XRD) and direct current (dc) conductivity measurements were used to survey the functionality of two pyrochlore-perovskite binary systems as high-temperature proton conductors (HTPCs). An efficient HTPC could be used in a number of electrochemical devices, such as gas separation membranes, fuel cells, or sensors. The primary driver for HTPC development is the need for hydrogen (H) separation membranes that can provide an unadulterated H stream from a reformate feed for coal gasification and petrochemical processes. Equally important, though, are the advantages an efficient HTPC could provide to a future generation of fuel cell technology.

A solid ceramic ion transport membrane has the greatest potential for producing pure H at high temperatures. Nafion membranes produced by DuPont (Wilmington, DE) are currently the most effective low-temperature proton conductors; however, their maximum operating temperature (~160 °C for hybrid membranes) is below the desired operating temperature (500-600 °C) for coal gasification.[1] Microporous membranes operate in this temperature range with high fluxes; however, they are at best 99% selective to H.[2] Ceramic membranes operate well at high temperatures and can be very selective; however, they are intolerant to H_2S and CO_2 contaminants and their flux is too low for practical application.[2, 3]

Ionic conductivity in ceramics can be enhanced by disorder. Typically, disorder is related to structural defects, such as oxygen vacancies, or to configurational features, such as the rotation and tilting of oxygen polyhedra. However, disorder can also be created by fluctuations in the crystal structure. Displacive properties, such as piezoelectricity, are enhanced at compositions near a phase boundary, where little separates one phase from another and localized regions can dynamically fluctuate between different crystal structures.[4] The inherent chaos of these structural fluctuations increases the kinetics of the system. It has recently been shown that transport properties can also be enhanced at a phase boundary, providing a new mechanism for developing fast ion conduction in ceramic oxides.[5]

Two pyrochlore-perovskite binary systems were studied. The crystal structure for pyrochlore, $A_2B_2O_7$, has octahedrally coordinated B-site cations, 8-coordinated A-site cations, and two distinct oxygen sites. The crystal structure of perovskite, ABO_3, also has octahedrally coordinated B-site cations, as well as 12-coordinated A-site cations. The pyrochlore-perovskite binary system was chosen because their crystal structures share several features, such as BO_6 octohedra. Additionally, small, localized regions of pyrochlore-type ordering were recently observed in perovskite materials.[6] Therefore, it was anticipated that compositions near the phase boundaries in these systems might exhibit enhanced conductivity due to structural fluctuations.

The pyrochlore $La_2Zr_2O_7$ and the perovskites $LaYO_3$ and $SrZrO_3$ were chosen for investigation because all have demonstrated proton conduction,[7-10] though their conductivity is low. Furthermore, all systems are stable in the presence of CO_2 and H_2S. Samples were tested across a full compositional range, thereby including doped-pyrochlore regions, doped-perovskite regions, near-phase boundary regions, and pyrochlore-perovskite heterophase mixtures.

2. Experimental Procedures

The glycine-nitrate process was used to produce powders of the test compositions.[11] Aqueous nitrate solutions of the ap-

This paper was presented at the Fuel Cells: Materials, Processing, and Manufacturing Technologies Symposium sponsored by the Energy/Utilities Industrial Sector & Ground Transportation Industrial Sector and the Specialty Materials Critical Technologies Sector at the ASM International Materials Solutions Conference, October 13-15, 2003, in Pittsburgh, PA. The symposium was organized by P. Singh, Pacific Northwest National Laboratory, S.C. Deevi, Philip Morris USA, T. Armstrong, Oak Ridge National Laboratory, and T. Dubois, U.S. Army CECOM.

Scott A. Speakman, Robert D. Carneim, E. Andrew Payzant, and **Timothy R. Armstrong,** Oak Ridge National Laboratory, Metals & Ceramics Division, Oak Ridge, TN 37831-6064. Contact e-mail: speakmansa@ornl.gov.

propriate cations were mixed with glycine fuel. Heat was used to evaporate the solvent until the fuel ignited, producing an as-burned powder. The as-burned powder was calcined at 900 °C for 1 h. The calcined powders were pressed into 12.7 mm diameter pellets and sintered at either 1000 °C for 96 h, 1500 °C for 2 h, or 1500 °C for 15 h. The compositions were

$(La_{1-x}Sr_x)ZrO_{3.5-x/2}$, $x = 0, 0.125, 0.25, 0.375, 0.5, 0.625, 0.75, 0.875, 1.0$,

$La(Zr_{1-x}Y_x)O_{3.5-/2}$, $x = 0, 0.04, 0.08, 0.125, 0.19, 0.25, 0.375, 0.5, 0.625, 0.75, 0.875, 1.0$.

XRD was used to analyze the as-burned, calcined, and sintered powders. XRD patterns were collected using Cu K_α radiation with a Scintag PADV and/or a Panalytical (Almelo, The Netherlands) X'Pert Pro diffractometer. Lattice parameters were determined by collecting an XRD pattern from the sintered powder intimately mixed with a National Institute of Standards and Technology (NIST) standard reference material (SRM). NIST 640c, Si, was used to calibrate samples consisting predominantly of perovskite phases; NIST 660a, LaB_6, was used to calibrate samples consisting predominantly of pyrochlore phases. Peak positions were determined by profile fitting individual diffraction peaks with pseudo-Voigt functions. The peak positions of the SRMs were used for internal 2θ calibration of the diffraction data.[12] The calibrated peak positions of the sample were analyzed with a cell refinement algorithm to determine the unit cell lattice parameters.[13]

Disks sintered at 1500 °C for 2 h were used for conductivity measurements. Four Pt-Rh electrode wires were attached with silver ink around the circumference of the disks with approximately even spacing and then were sintered at 900 °C. The electrical conductivities were measured in air at temperatures of 300-900 °C using a four-point van der Pauw technique.[14] Electronic measurements were made with two Keithley 6517A (Cleveland, OH) electrometers and an Agilent 34970A (Palo Alto, CA) switch unit. One electrometer simulated a current source, applying voltages (V_{appl}) of ±10, 5, 2.5, 1.25, and 0.675 V and measuring the corresponding current (I_{source}) across two electrodes; while the second electrometer measured the resulting potential (V_{obs}) across the two parallel electrodes. The ten measurements made at different V_{appl} were analyzed for linearity and consistency. The linear portion of the $I_{source}V_{obs}$ curve was then used to determine the resistance. These measurements were repeated for 4 configurations of the electrodes M, N, O, and P: $I_{MN}V_{OP}$, $I_{NO}V_{PM}$, $I_{OP}V_{MN}$, and $I_{PM}V_{NO}$. The measurements of $I_{MN}V_{OP}$ and $I_{OP}V_{MN}$ were averaged together to produce R_A; likewise, $I_{NO}V_{PM}$ and $I_{PM}V_{NO}$ were averaged together to produce R_B. The resistivity (ρ) was then solved from the equation:

$$\exp\left(-\frac{\pi d}{\rho}R_A\right) + \exp\left(-\frac{\pi d}{\rho}R_B\right) = 1 \quad \text{(Eq 1)}$$

where d is the thickness of the pellet. These measurements were performed in a Thermolyne F21130-33 (Dubuque, IA) tube furnace at different temperatures. The sample temperature was measured with a thermocouple that was independent from the one used to operate the furnace. The resulting temperature and conductivity data were used in an Arrhenius analysis to determine the activation energy (E_A) and pre-exponential geometric factor (σ_o) according to the equation:

$$\sigma_{ion} = \frac{\sigma_o}{T}\exp\left(-\frac{E_A}{kT}\right) \quad \text{(Eq 2)}$$

Table 1 Activation Energies and Geometric Pre-Exponential Factors Calculated from Arrhenius Analysis of Electrical Conductivity in Air

Composition	Activation Energy, eV	log σ_0, K, S/cm	Conductivity at 600 °C, $\times 10^{-5}$ S/cm
$SrZrO_3$	0.466	4.008	0.75
$La_{0.125}Sr_{0.875}ZrO_{3.0625}$	0.520	4.119	0.18
$La_{0.25}Sr_{0.75}ZrO_{3.125}$	0.424	3.539	0.92
$La_{0.375}Sr_{0.625}ZrO_{3.1875}$	0.389	3.580	2.98
$La_{0.5}Sr_{0.5}ZrO_{3.25}$	0.393	3.960	6.18
$La_{0.75}Sr_{0.25}ZrO_{3.375}$	0.372	4.146	18.3
$La_{0.875}Sr_{0.125}ZrO_{3.4375}$	0.363	4.149	24.2
$LaZrO_{3.5}$	0.376	3.712	5.91
$LaZr_{0.96}Y_{0.04}O_{3.48}$	0.335	3.841	28.1
$LaZr_{0.92}Y_{0.08}O_{3.46}$	0.351	4.016	25.5
$LaZr_{0.875}Y_{0.125}O_{3.4375}$	0.387	4.427	21.7
$LaZr_{0.75}Y_{0.25}O_{3.375}$	0.404	4.503	15.7
$LaZr_{0.625}Y_{0.375}O_{3.3125}$	0.435	4.646	8.50
$LaZr_{0.5}Y_{0.5}O_{3.25}$	0.437	4.479	5.46
$LaZr_{0.375}Y_{0.625}O_{3.1875}$	0.471	4.460	1.83
$LaZr_{0.25}Y_{0.75}O_{3.125}$	0.544	5.030	0.72
$LaZr_{0.125}Y_{0.875}O_{3.0625}$	0.536	4.642	0.38
$LaYO_3$	0.431	4.609	8.64
$La_{0.95}Y_{0.05}ZrO_{3.5}$	0.390	4.148	10.5

The conductivity at 600 °C was calculated from the latter two values using Eq. 2.

3. Results

Table 1 lists the activation energies, geometric factors, and conductivities at 600 °C for the samples that were tested. The E_A and σ_o were determined by linear regression analysis of the observed conductivity data. The conductivity at 600 °C was calculated from Eq 2 using the values for E_A and σ_o in Table 1. Figure 1 shows the electrical conductivity for the various compositions in air at 600 °C, while Fig. 2 shows the variation of E_A and σ_o with composition.

The conductivities of both $(La_{1-x}Sr_x)ZrO_{3.5-x/2}$ and $La(Zr_{1-x}Y_x)O_{3.5-x/2}$ varied similarly with composition. Low levels of doping in $La_2Zr_2O_7$, whether by the substitution of Sr for La or the substitution of Y for Zr, produced a modest increase in the high-temperature conductivity. Likewise, both $(La_{1-x}Sr_x)ZrO_{3.5-x/2}$ and $La(Zr_{1-x}Y_x)O_{3.5-x/2}$ exhibited a depression in conductivity at low levels of doping in the perovskite phase, whether La-doped $SrZrO_3$ or Zr-doped $LaYO_3$. The conductivities of compositions $0.125 < x < 0.875$ varied almost linearly and empirically appeared to be a mixing function of the conductivity at $x = 0.125$ and $x = 0.875$.

Though the conductivities of $(La_{1-x}Sr_x)ZrO_{3.5-x/2}$ and $La(Zr_{1-x}Y_x)O_{3.5-x/2}$ behaved similarly, their dopant solubilities did not. In $(La_{1-x}Sr_x)ZrO_{3.5-x/2}$, a phase pure product was only formed for $x = 0$ and 1. All other compositions produced heterophase mixtures of perovskite and pyrochlore phases. By

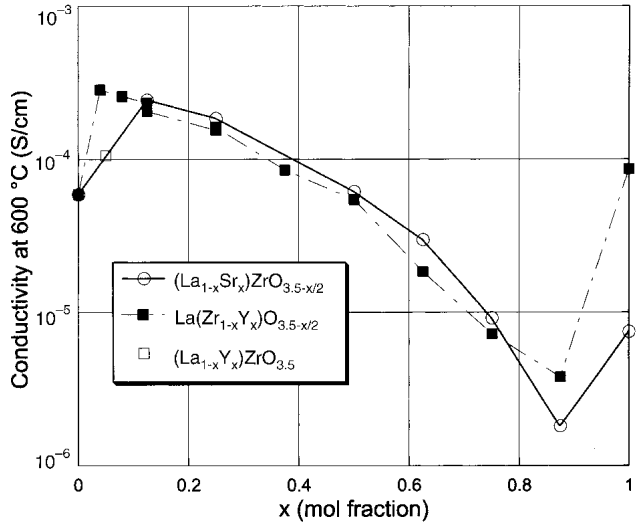

Fig. 1 Electrical conductivity at 600 °C in air, as calculated from Eq 2 using the values listed in Table 1

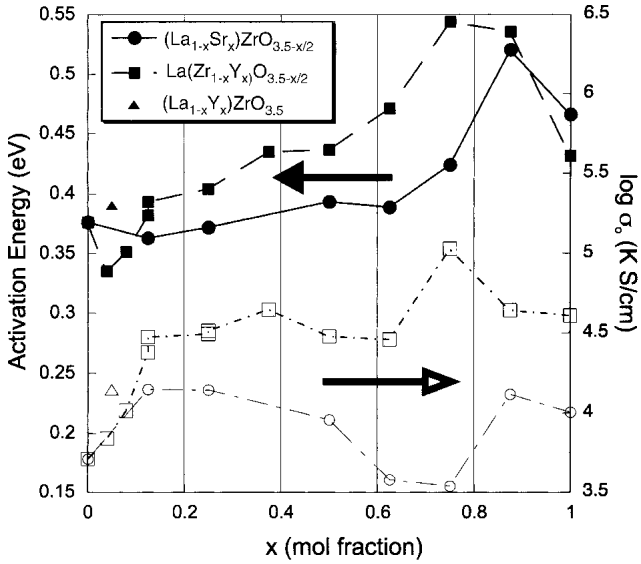

Fig. 2 Activation energies (solid data points) and geometric pre-exponential factors (hollow data points) for electrical conductivity, as determined by Arrhenius analysis of dc conductivity data

contrast, in $La(Zr_{1-x}Y_x)O_{3.5-x/2}$ a phase pure perovskite was formed when $x = 1$ and 0.875 and a phase pure pyrochlore was formed at compositions between $0 \leqslant x \leqslant 0.25$.

Figure 3 illustrates that the lattice parameters of $(La_{1-x}Sr_x)ZrO_{3.5-x/2}$ did not vary with composition for either the pyrochlore or perovskite phases. This indicated that little or no doping occurred. However, the variations in conductivity observed in Fig. 1 empirically suggested that some small level of doping, perhaps below the detection level of XRD analysis, occurred. Alternatively, conductivity may have been affected by an interfacial interaction between pyrochlore and perovskite phases; however, there was no strong evidence to support this hypothesis.

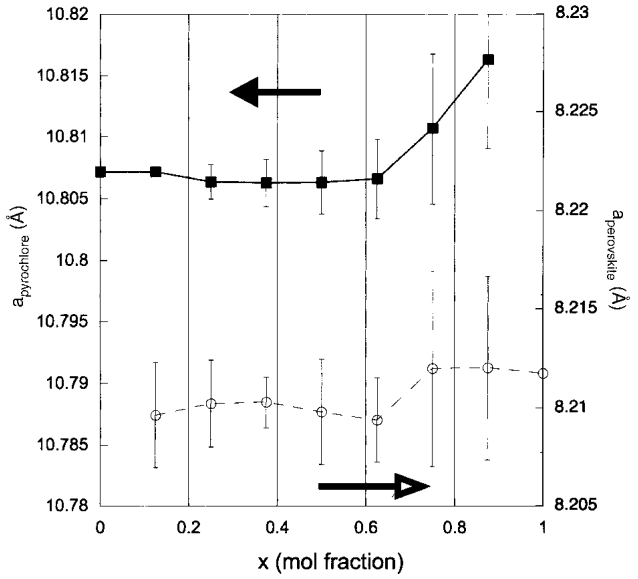

Fig. 3 Variation of the lattice parameters of pyrochlore (solid data points) and perovskite (hollow data points) phases formed in $(La_{1-x}Sr_x)ZrO_{3.5-x/2}$. Error bars are estimated standard deviations calculated by the cell refinement algorithm. The apparent increase in the pyrochlore lattice parameter at $x > 0.625$ was an artifact resulting from the low quantity of pyrochlore phase producing weak diffraction peak intensities.

The $La(Zr_{1-x}Y_x)O_{3.5-x/2}$ phase diagram is more complicated than that of $(La_{1-x}Sr_x)ZrO_{3.5-x/2}$, despite the similarities in their conductivities. A pyrochlore phase formed at $0 \leq x \leq 0.25$ for $La(Zr_{1-x}Y_x)O_{3.5-x/2}$, though a small amount of La_2O_3 impurity was observed when $x = 0.125$ and 0.19 and an unidentified phase was observed when $x = 0.25$. Examination of lattice parameters, shown in Fig. 4, revealed that Y did not substitute only for Zr as anticipated, but rather substituted for both Zr and La at higher doping levels. According to Vegard's Law, if the substitution of Y into $La_2Zr_2O_7$ followed a consistent pattern then the variation of the lattice parameter with composition would be linear. The lattice parameters of tested compositions between $0 \leqslant x \leqslant 0.25$ were not collinear, but rather demonstrated a discontinuity between $x = 0.08$ and 0.125. In Fig. 4, the lattice parameter of $(La_{0.95}Y_{0.05})ZrO_{3.5}$ is also shown; it was significantly smaller than that of $La_2Zr_2O_7$. These data supported a hypothesis that Y substitutionally doped both the A and B sites. The substitution of La with the smaller Y cation on the A-site produced a smaller unit cell in $(La_{0.95}Y_{0.05})ZrO_{3.5}$, while the substitution of Zr with the larger Y cation on the B-site produced a larger unit cell in $La(Zr_{0.96}Y_{0.04})O_{3.48}$. At $x = 0.125$, 0.19, and 0.25, Y substituted onto both the A- and B-sites, producing a mixed effect on the size of the unit cell. This hypothesis was further supported by the observation of La_2O_3 in the XRD patterns of $x = 0.125$ and 0.19, shown in Fig. 5. Since the composition was formulated for pure B-site substitution, the occupancy of Y on the A-site produced excess La_2O_3. The lack of La_2O_3 in the XRD pattern of $x = 0.25$ deviated from this hypothesis; however, there was a second phase observed that was not identified. It was suggested that this phase was a La-rich phase that formed instead of La_2O_3,

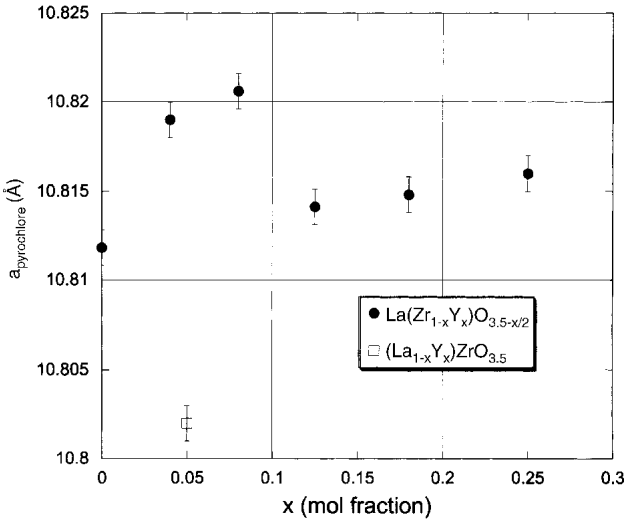

Fig. 4 Variation of the lattice parameter of the pyrochlore phase in $La(Zr_{1-x}Y_x)O_{3.5-x/2}$. Error bars represent 0.001 Å, which was the average standard deviation for all cell refinements.

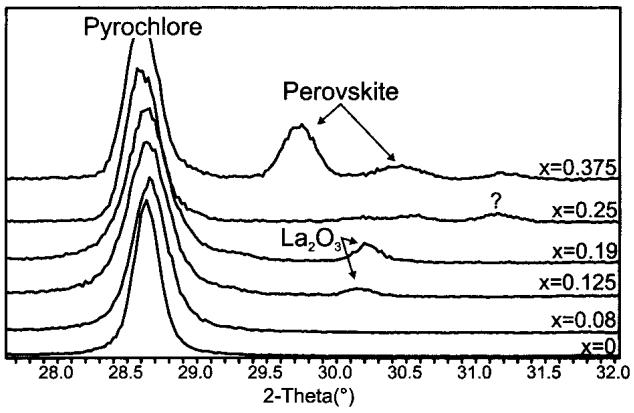

Fig. 5 XRD patterns for $La(Zr_{1-x}Y_x)O_{3.5-x/2}$ at $x \leq 0.375$, showing the formation of secondary phases

though this was not definitively proven. The exact composition at which Y began to substitute onto the A-site was not clearly identified. The lattice parameter of $x = 0.08$ lies below a line defined by the lattice parameters at $x = 0$ and $x = 0.04$, suggesting that the lattice parameter at $x = 0.08$ was not as large as it would be if Y substituted only for Zr on the B-site and therefore that a small amount of A-site substitution may have occurred at $x = 0.08$.

As a consequence of the A-site substitution by Y, the electrical conductivity did not increase above its level at $x = 0.04$ and 0.08. The substitution of La with Y did not produce oxygen vacancies, and therefore had little effect on the conductivity. The substitution of Y for Zr in $La_2Zr_2O_7$ at 0.04 and 0.08 mol fraction increased σ_o and decreased E_A, thereby increasing the overall conductivity; however, the Y-doping at greater levels of 0.125, 0.19, and 0.25 mol fraction consisted mostly of La substitution and consequently increased E_A, leading to a decrease in conductivity.

The conductivity behavior of $La(Zr_{1-x}Y_x)O_{3.5-x/2}$ at $x \geq$

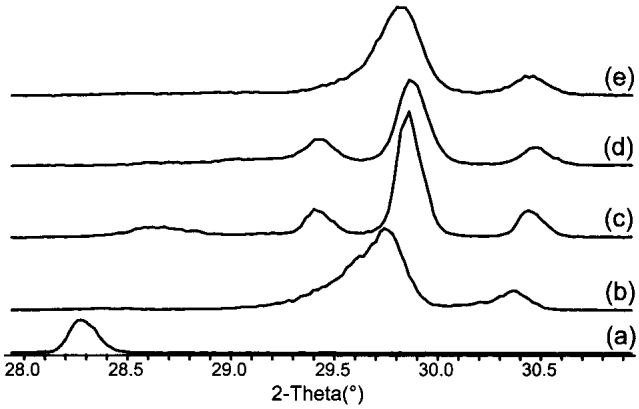

Fig. 6 XRD patterns of $La(Zr_{0.125}Y_{0.875})O_{3.0625}$ from: **(a)** surface of a pellet sintered at 1500 °C; **(b)** interior of a pellet sintered at 1500 °C (surface layer was ground away); **(c)** pellet sintered at 1000 °C (representative of surface and interior); **(d)** pellet not ground, tested in dc conductivity measurement, then ground and tested again; **(e)** pellet that was ground, tested in dc conductivity measurement, then reground and tested again

0.875 paralleled that of $(La_{1-x}Sr_x)ZrO_{3.5-x/2}$, but the phase composition was markedly different, showing a dependence on thermal history, as illustrated in Fig. 6. Samples sintered at 1000 °C were an orthorhombic polymorph of $LaYO_3$.[15] Pellets sintered at 1500 °C had different phases on the surface and within the interior of the pellet. The surface phase was a metastable cubic polymorph of $LaYO_3$,[16] while the interior of the pellet was an unindexed polymorph of $LaYO_3$, hereafter referred to as the O′ phase. The O′ phase was best described with an orthorhombic unit cell, similar to the orthorhombic polymorph formed at 1000 °C but with an *a/b* ratio closer to 1 (i.e., more nearly tetragonal) and a different symmetry. A definitive indexing was not achieved. To test the effect of these polymorphs on conductivity, two pellets of $La(Zr_{0.125}Y_{0.875})O_{3.0625}$ were sintered at 1500 °C. One pellet was ground to remove the surface layers, then electroded; the unground surfaces of the other pellet were electroded. After in situ dc conductivity measurements were collected up to 900 °C, both samples were ground, electroded, and then tested again. The resulting Arrhenius plots are shown in Fig. 7, and the conductivity data are reported in Table 2. The sample that was initially ground and tested, then reground and tested again, showed consistent conductivity behavior. However, the sample that was not ground initially showed a large deviation in conductivity behavior between the two tests (unground and then ground) and as compared with the ground sample. The data in Table 2 show that the conductivity of the unground sample was lower than that of the ground sample due to the significantly larger activation energy. This empirically indicated that the cubic phase of the surface layer acted as a barrier to conduction. After the sample that was initially unground was ground and tested again, it showed a large change in conductivity. The conductivity no longer followed an Arrhenius behavior and showed a large hysteresis. Though only one data set is shown in Fig. 7, these results were repeatable. XRD analysis revealed differences between these samples, as shown in Fig. 6. The pellet that was not ground initially consisted of the cubic polymorph as a surface

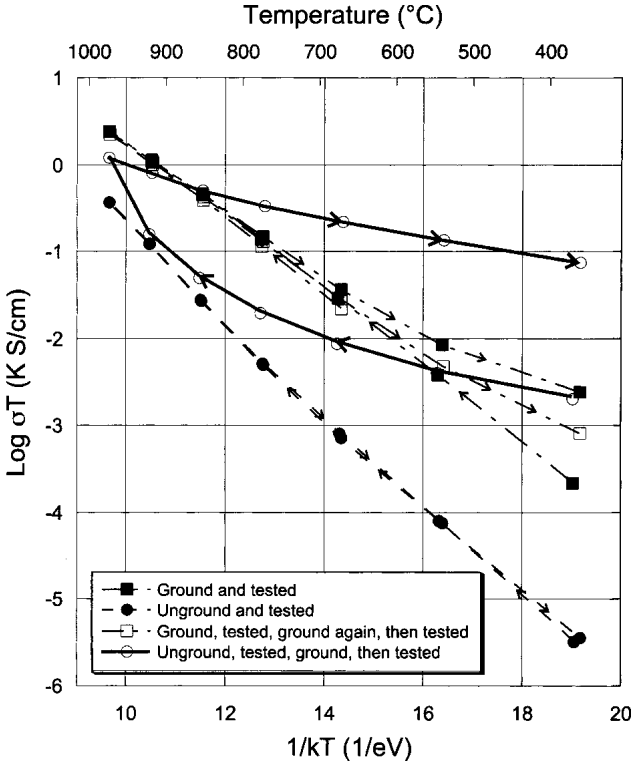

Fig. 7 Arrhenius plots from $La(Zr_{0.125}Y_{0.875})O_{3.0625}$ samples that were ground and not ground, then tested in dc conductivity measurement in air; then ground and tested again

Table 2 Activation Energies and Pre-Exponential Geometric Factors Calculated from Arrhenius Analysis of Conductivity Data for $La(Zr_{0.125}Y_{0.875})O_{3.0625}$ Samples with Different Preparation Histories and the Conductivities Calculated from the Latter Two Values Using Eq 2

History	Activation Energy, eV	log σ_0, K S/cm	Conductivity at 600 °C $\times 10^{-5}$ S/cm
Unground and tested	0.536	4.642	0.38
Unground, tested, then ground and tested again (a)	0.267(a)	2.022(a)	3.43(a)
Ground and tested	0.433	4.609	8.23
Ground, tested, then ground and tested again	0.432	4.548	7.35

(a) These values are only approximate because of the nonlinearity of the conductivity data, as illustrated in Fig. 7.

layer and the O′ polymorph as a bulk interior phase, while the sample that was ground contained only the O′ phase. After the two sets of conductivity measurements, the sample that was initially ground retained the O′ phase, while the sample that was not initially ground had transformed into the orthorhombic polymorph of $LaYO_3$. XRD data were not collected between the two conductivity tests, so the point at which the unground sample transformed from the O′ to the orthorhombic phase was not identified. However, the impact of the polymorphism of $LaYO_3$ on conductivity was confirmed.

4. Summary

Doping of $La_2Zr_2O_7$, $LaYO_3$, and $SrZrO_3$ was shown to affect the electrical conductivity. The substitutional doping of Sr for La and Y for Zr in $La_2Zr_2O_7$ increased the conductivity, with the greatest gains achieved by 4 and 8 mol% substitution of Y for Zr. Yttrium was more soluble in $La_2Zr_2O_7$ than Sr; however, its effectiveness as a dopant was hindered by its tendency to substitute for both A- and B-site cations at higher doping levels. Neutron and x-ray powder diffraction data have been collected for Rietveld refinement of these systems. These data will facilitate more exact identification of site occupancies in these systems and a greater understanding of the relationship between structure and conductivity.

The enhancement of conductivity at phase boundaries was not demonstrated. This may have been due to several reasons, but primarily owing to the lack of miscibility between the chosen systems. It may also have been caused by the occupancy of Y on both A- and B-sites in $La_2Zr_2O_7$, which precluded a single, well-defined phase boundary between pyrochlore and perovskite phases. The complex system of polymorphs of $LaYO_3$-based perovskites may also have hindered the dynamics near the phase boundary. Computer simulation of empirical potential models is currently being used to identify pyrochlore-perovskite binary systems with greater miscibility and therefore a greater chance of producing enhancement of the conductivity near the phase boundaries.

Acknowledgments

Research sponsored by the Laboratory Directed Research and Development Program of Oak Ridge National Laboratory (ORNL), managed by UT-Battelle, LLC for the U. S. Department of Energy under Contract No. DE-AC05-00OR22725.

References

1. G. Alberti and M. Casciola: "Solid State Protonic Conductors, Present Main Applications and Future Prospects," *Solid State Ionics*, 2001, *145*(1-4), pp. 3-16.
2. Y.S. Lin: "Microporous and Dense Inorganic Membranes: Current Status and Prospective," *Separation and Purification Technology*, 2001, *25*(1-3) pp. 39-55.
3. R.D. Carneim and T.R. Armstrong: "Decomposition of Yttrium-Doped Barium Cerate in Carbon Dioxide," *J. Am. Chem. Soc*, 2003, in press.
4. R. Newnham: "Phase Transformations in Smart Materials," *Acta Crystallogr.*, 1998, *A54*(6.1) pp. 729-37.
5. H. Yamamura, H. Nishino, K. Kakinuma, and K. Nomura: "Electrical Conductivity Anomaly Around Fluorite-Pyrochlore Phase Boundary," *Solid State Ionics*, 2003, 158(3-4) pp. 359-65.
6. J. Irvine: "High Temperature Fuel Cell Materials-Structure at Ion's Length," presented at *Materials for Energy Production and Storage Conference*, Rutherford Appleton Laboratory, 6-7 March 2003.
7. J.A. Labrincha, J.R. Frade, and F.M.B. Marques: "Protonic Conduction in $La_2Zr_2O_7$-based Pyrochlore Materials," *Solid State Ionics*, 1997, *99*(1-2) pp. 33-40.
8. E. Ruiz-Trejo and J.A. Kilner: "Oxygen Diffusion and Proton Conduction in $La_{1-x}Sr_xYO_{3-d}$," *Solid State Ionics*, 1997, *97*(1-4) pp. 529-34.

9. J.A. Labrincha, F.M.B. Marques, and J.R. Frade: "Protonic and Oxygen-Ion Conduction in $SrZrO_3$-Based Materials," *J. Mater. Sci.*, 1995, *30*(11) pp. 2785-92.
10. T. Schober, F. Krug, and W. Schilling: "Criteria for the Application of High Temperature Proton Conductors in SOFCs," *Solid State Ionics*, 1997, *97*(1-4) pp. 369-73.
11. L.A. Chick, L.R. Pederson, G.D. Maupin, J.L. Bates, L.E. Thomas, and G.J. Exarhos: "Glycine-Nitrate Combustion Synthesis of Oxide Ceramic Powders," *Mater. Lett.*, 1990, *10*(1-2) pp. 6-12.
12. R. Jenkins and R.L. Snyder, *Introduction to X-Ray Powder Diffractometry*, John Wiley & Sons, New York, New York, 1996, pp. 281-5.
13. Materials Data, Inc., *Jade v. 6.5.5*, Livermore, CA, 2003.
14. L.J. van der Pauw: "A Method of Measuring the Resistivity and Hall Coefficient on Lamellae of Arbitrary Shape," *Philips Technical Review*, 1958, *20*(8) pp. 220-4.
15. J. Coutures and M. Foex: "Etude à Haute Température du Diagramme d'Equilibre du Système Formé par le Sesquioxyde de Lanthane avec le Sesquioxyde d'Yttrium, " *J. Solid State Chem.*, 1974, *11*(4) pp. 294-300 (in French).
16. O. Yamaguchi, H. Kawabata, H. Hashimoto, and K. Shimizu: "New Modification of $LaYO_3$," *J. Am. Ceram. Soc.*, 1987, *70*(6), pp. C131-32.